Doctoral Dissertation (Censored)

博士論文（要約）

New hydrogen-ordered phase and proton dynamics of ice revealed by dielectric and neutron diffraction measurements using newly developed high pressure cells

（誘電率および中性子回折測定用の高圧セル開発による
氷高圧相の新しい秩序相の発見とプロトンダイナミクスの解明）

A Dissertation Submitted for the Degree of Doctor of Philosophy
December 2019
令和元年 12 月　博士（理学）申請

Department of Chemistry, Graduate School of Science,
The University of Tokyo
東京大学大学院理学系研究科
化学専攻

Ryo Yamane
山根　崚

Abstract

Ice is the most fundamental molecular solid in the large material group, such as confined water and hydrates, characterized by water molecules. Nineteen ice polymorphs have been reported so far. The polymorphs can be classified into hydrogen-disordered and hydrogen-ordered phases, where hydrogen atoms occupy their sites at 50 and 100%, respectively. These states include some notable physical phenomena, such as a residual entropy caused by ice rule. In this thesis, I studied two unresolved problems of disordered high-pressure phases, ice VI and VII appearing at 1–2 GPa and 2–60 GPa, respectively. Salzmann *et al.* (2009) found that impurity-doping induces a phase transition to its ordered phase, ice XV, using neutron diffraction. Recently, the existence of another ordered phase was suggested in addition to ice XV (Gasser *et al.*, 2018). Anomalous behavior of ice VII, on the other hand, has been reported around 10 GPa. For example, Pruzan *et al.* (1990) reported that a width of a Raman band of a symmetric stretching mode of a water molecule, has a minimum at around 10 GPa. Somayazulu *et al.* (2008) showed a peak splitting in an X-ray diffraction pattern at 14.8 GPa. Okada *et al.* (2014) showed that DC electric conductivity of ice VII has a maximum at 12 GPa from impedance measurements. However, no comprehensive interpretation for the experimental anomalies has been found.

Chapter **2** describes the discovery of a new hydrogen-ordered phase of ice VI, named as ice XIX, from *in situ* of dielectric and neutron diffraction measurements at high pressure. Ice XV has been known as a hydrogen-ordered phase of ice VI so far. This is the second discovery of hydrogen-ordered phase of ice VI. Representative data of temperature dependence of dielectric loss and neutron diffraction of ice VI and ice XIX are shown in Fig. 1. Hydrogen ordering was observed as disappearance of dielectric response at 117 K (Fig. 1(a)) and as appearance of new peaks in the diffraction pattern at 108 K (Fig. 1(b)). These phenomena were caused by a limitation of reorientation of water molecules and symmetry lowering accompany with the hydrogen-ordering. Furthermore, structure analysis of ice XIX clarified that its unit cell is expanded to $\sqrt{2} \times \sqrt{2} \times 1$ from a unit cell of ice VI. I also proposed the two most possible structure models for ice XIX whose space groups are $P\overline{4}$ and $Pcc2$.

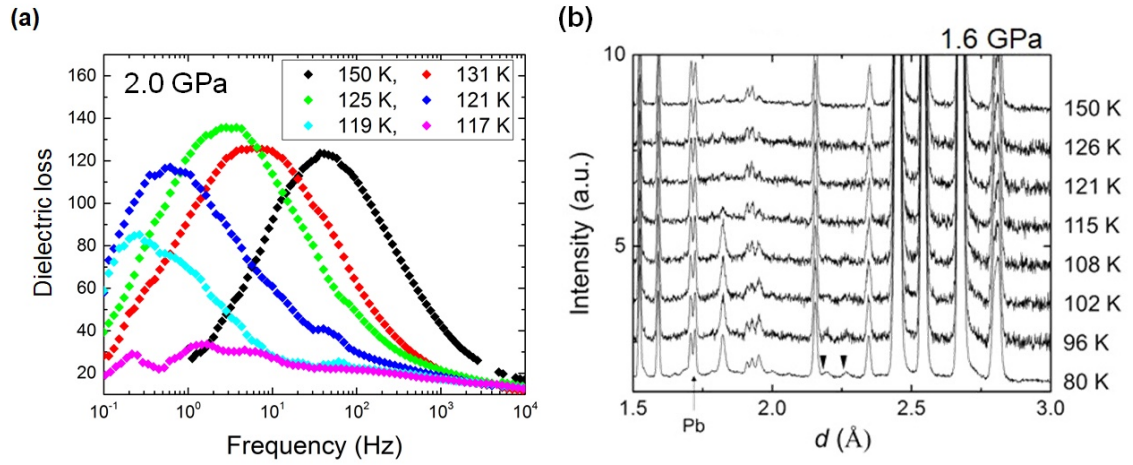

FIG. 1: (a) Temperature dependence of dielectric loss of ice VI and its new ordered phase at 2.0 GPa. (b) Neutron diffraction patterns obtained at 1.6 GPa and temperatures between 80–150 K. Pb, pressure marker, shows a peak at around 1.75 Å. The black triangle ticks indicate that their corresponding peaks are derived from $\sqrt{2} \times \sqrt{2} \times 1$ unit cell of a new ordered phase of ice VI. Hydrogen disorder-order transition can be seen at around 120 K in both measurements.

Chapter **3** describes investigation of dielectric properties of ice VII beyond 10 GPa using a newly developed high-pressure cell. As a result, a theoretically predicted scenario was observed (Hernandez and Caracas, 2018); dominant dynamics of disordered state of ice VII changes from molecular rotation to proton translation at around 10 GPa. Figure 2 shows the dynamics crossover observed in my dielectric experiments. Two dielectric relaxations were observed below 8.6 GPa, and the expected pressure response was observed considering activation volume of the each dynamics; molecular rotation was inactivated and proton translation was activated with increasing pressure. The two dielectric relaxations merged at around 10 GPa on the frequency axis, and the dielectric relaxation of proton translation is faster than that of water rotation above the pressure. This result is the direct observation of the theoretically predicted dynamics crossover in ice VII. My study gives the solution to the reported anomalous behavior of ice VII

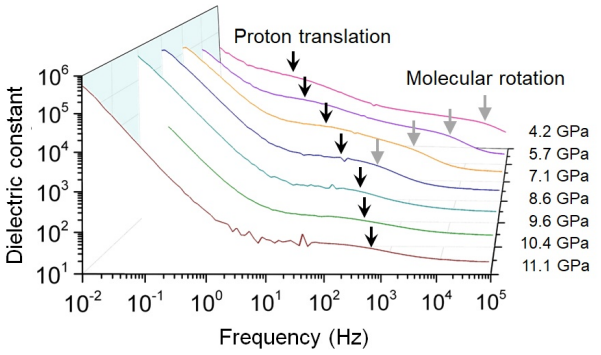

FIG. 2: Pressure dependence of dielectric constant of ice VII. Black and grey arrows indicate dielectric relaxations with their dynamics.

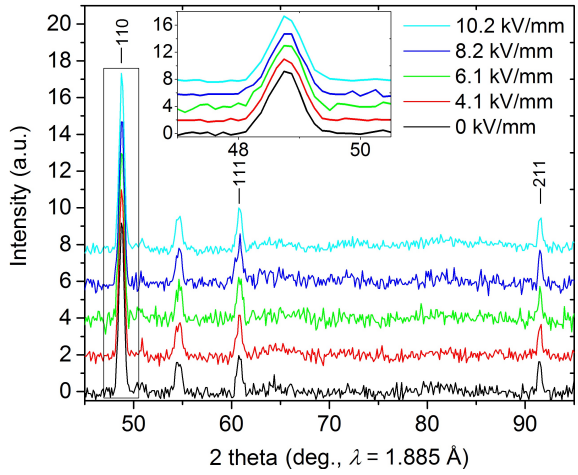

FIG. 3: Neutron diffraction patterns at 6.2 GPa and with electric fields of 0, 4.1, 6.1, 8.2, and 10.2 kV/mm. Exposure times were 1, 1, 0.5, 0.5, and 2 h, respectively. The inset shows expanded plots at around 50°. From lower angle, 110, 111, and 211 reflections of ice VII are observed. The peak at around 55° is 110 reflection of diamond (anvils). The undulation from 60° to 90° could be derived from inhomogeneous gaps of the radial-collimator partitions.

at around 10 GPa with the theoretical report (Hernandez and Caracas, 2018).

Chapter **4** describes neutron diffraction experiments of ice VII carried out under high pressure and high electric field for search of a ferroelectrically (abbreviated FE) ordered structure of ice VII. Coexistence of FE ordered domain in ice VII was also theoretically suggested as an interpretation for the anomalous behavior of ice VII at around 10 GPa (Caracas and Hemley, 2015). This is the first case of neutron experiments under the multi-extreme conditions. As a result, no clear evidence of the appearance of the FE ordered structure of ice VII was obtained from the observed diffraction patterns as shown in Fig. 3. Although further technical improvements would be necessary to find the potential existence FE structure, this study will be continued for the aim of the discovery of FE ordered structure by applying much higher electric field. The discovery should have a high impact considering its notable structural property in contrast to a typical antiferroelectrically ordered structure, ice VIII, which is an ordered phase of ice VII.

Chapter **5** describes technical developments for high-pressure dielectric experiments. Figure 4(a) and (b) show the two developed cells. These cells are used depending on target pressures; one of them is a piston-cylinder type and the other one is a Bridgman type cell. Their achievable pressures are up to 2.5 GPa and 13 GPa, respectively. Sample pressure can be estimated from *in situ* ruby fluorescence measurement. A notable feature of the cells is that they are applicable to not only solid samples but also liquid samples by overcoming technical difficulties, such as maintaining electrodes in parallel under high pressure.

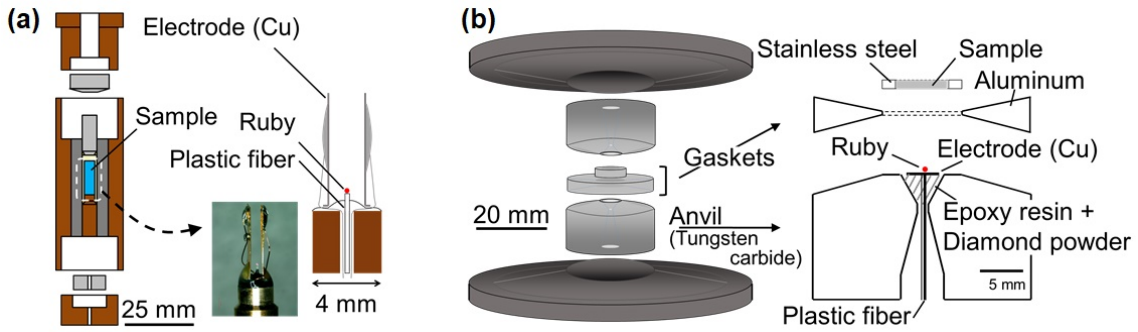

FIG. 4: Cell assemblies of piston-cylinder and Bridgman type high-pressure apparatuses for dielectric measurements, shown in (a) and (b), respectively. Samples are loaded vertically and their pressures are estimated using ruby fluorescence method.

In conclusion, I clarified the two unresolved problems of high-pressure phases of ice, VI and VII using newly developed high-pressure cells. I found the new ordered phase of ice VI besides the known ordered phase, ice XV. This is the first study revealing that one disordered ice has two hydrogen-ordered phases. This one-to-many correspondence opens new avenues to investigate the diversity of ice. For the anomalous behavior of ice VII at around 10 GPa, I directly observed that dominant dynamics of disordered state of ice VII changes from molecular rotation to proton translation. The first observation of the proton dynamics gives an experimental insight in light of its pressure response for not only ice but also other substances, such as proton conductors. As a different approach for the anomalous behavior of ice VII, I studied the search for a FE ordered structure of ice VII using neutron diffraction under high pressure and high electric field. Although I have not found out the FE ordered structure yet, my original experiment motivates other future works aiming to open a new research field of ice using electric field, such as an electric field induced new phase of ice.

Contents

1 General Introduction

Ice is the most fundamental molecular solid in the large material group, such as confined water and hydrates, characterized by water molecules. Water molecules and their hydrogen-bond networks make various crystal forms of ice [1]. Twenty ice polymorphs have been discovered including this study so far, and they show notable electric properties derived from an electric dipole moment of a water molecule. The polymorphs can be classified into hydrogen-disordered and hydrogen-ordered phases [1], where hydrogen atoms occupy their sites at 50 and 100%, respectively. Some of hydrogen-ordered phases have ferro or antiferroelectrically ordered structures (e.g. [2–4]). In disordered states, on the other hand, the dipole moments have random orientations and they reorient their directions constantly by molecular rotation and proton translation. These dynamics cause a variety of dielectric response of disordered ice (e.g. [5–7]). Moreover, the proton dynamics also derives a notable electric characteristic of ice, proton conductivity [8]. Proton migration in hydrogen-bond networks of ice is known as Grotthuss mechanism [9], and the proton dynamics is extensively recognized in other proton conductors (e.g. [10]). Those electric characteristics, originated from a water molecule and hydrogen atom, have been focused in memory materials and electric conductors (e.g. [11–13]) with merits of abundance of H_2O and H. From the simple chemical composition of ice, it has given us deep or new insights of other substances including water molecules and hydrogen bonds even up to now and in the future. In this chapter, we start from a review on discovery history of ice polymorphs. This thesis reports a discovery of a new phase of ice, named ice XIX, and the historical review is helpful to understand what meanings this study has as a research direction of ice from now on. We also focus on previous studies of Ice Ih and its hydrogen ordering as an example of a hydrogen disorder - order phase transition, because all essential points of this thesis are found in the previous studies.

1.1 Historical review of ice polymorphs

"Ih" is the notation for the most famous ice polymorphs. The Roman numeral basically represents discovered order of its polymorphs besides such as ice Ic, which is a metastable disordered phase corresponding to ice Ih. The alphabets, h and c, are exceptionally given for ice Ih and Ic and they mean crystal system of each structure,

hexagonal and cubic, respectively. Discovery history of ice polymorphs has been accompany with experimental breakthrough so far; for example ice II and III were found by high-pressure technical developments by Percy Williams Bridgman in the beginning of 20th century [14], who is the father of high-pressure physics. Since his initial development, several ice polymorphs were found up to seventh ice, ice VII, with improvements of high-pressure techniques (see Fig. 1.1 and [15]). These discoveries are basically about hydrogen-disordered phase. Whalley and Davidson (1966) first reported a hydrogen-ordering phase transition from ice VII to ice VIII above 2 GPa at around 0°C [16]. Since their discovery, some ordered phases of ice were found up to fifteenth ice, ice XV [1], except for ice X and XII which are high pressure phase of ice VII appears above 60 GPa [17] and hidden disordered phase at around 1 GPa [18], respectively.

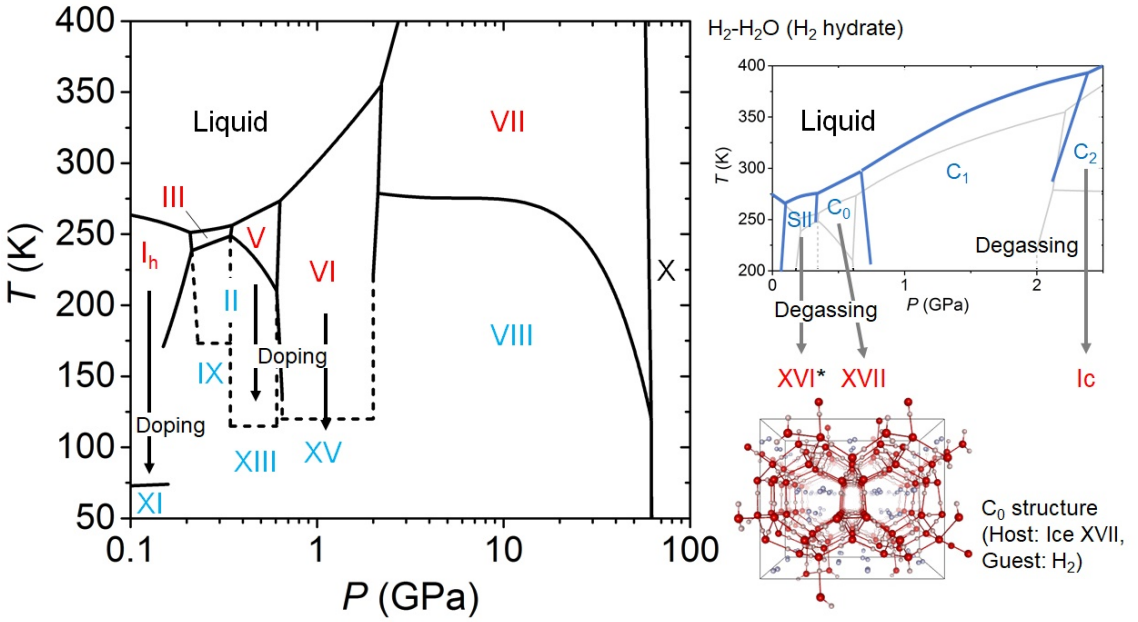

FIG. 1.1: Phase diagram of ice and H_2 hydrate. In the phase diagram of ice, red and light blue colored phases represent hydrogen disordered and ordered states, respectively. In ice X, atomic positions of hydrogen comes to the middle of hydrogen-bonded oxygen atoms, and the phase is written by black color. The dotted lines mean undetermined phase boundaries. The phase diagram of H_2 hydrate is overwritten on the phase diagram of ice for comparison. H_2 hydrate has some high-pressure phases, whose host structures are new ice phases. Ice XVI denoted asterisk was obtained the SII type structure, though the guest molecule was neon.

Among the discoveries of hydrogen-ordered phases, Kawada (1972) found an impurity-doping technique to induce hydrogen ordering from ice Ih to ice XI [19]. The technique has been extensively used for discoveries of new ordered phases of

ice [20]. My discovery of a new phase was achieved by a combination of the high-pressure technical developments and the impurity-doping technique. In addition, recently new disordered phases of ice were reported by strategic processes; ice XVI and XVII were made from degassing process of guest molecules put in ice XVI and XVII host cage ([21] and [22]). Ice XVIII was found as high-temperature and high-pressure phase of ice VII (above 2000 K and 100 GPa) by *in situ* X-ray diffraction measurements of laser-shocked water droplets [23].

1.2 Ice polymorphs and its diversity

Nineteen ice polymorphs have been reported so far, and the large number of polymorphs is a notable feature of ice. The diversity of ice polymorphs is mainly from two reasons: flexibility of a water molecule and hydrogen bond, and the hydrogen disorder-order phase relationship. The latter one is understood from the phase diagram of ice. In terms of the flexibility of water molecule, it is known from gas-phase studies that the H-O-H angle is 104.5°. On the other hand, the H-O-H angle shows large distribution in ice polymorphs. This distribution can be explained by low electron density of hydrogen atoms; the relatively low electron repulsion makes a water molecule bent its H-O-H angle easily. Fig. 1.2 shows the H-O-H angle distribution in some ice polymorphs. When we compress ice ih, the angle distribution is scattered with increasing pressure and the distribution has a maximum at ice V. It can be also seen in its complicated crystal structure (see Fig. 1.2). Beyond the pressure region of ice V, higher-pressure phases, ice VI and VII, make two independent hydrogen-bonded networks in their structures, which are denoted by blue and red-colored oxygen atoms in Fig. 1.2. These independent networks make the convergence of the angle distribution; water molecules can avoid making hydrogen bonds forcibly as like as ice V. Additionally, the flexibility of hydrogen bond also causes the variety of its networks among ice polymorphs [1].

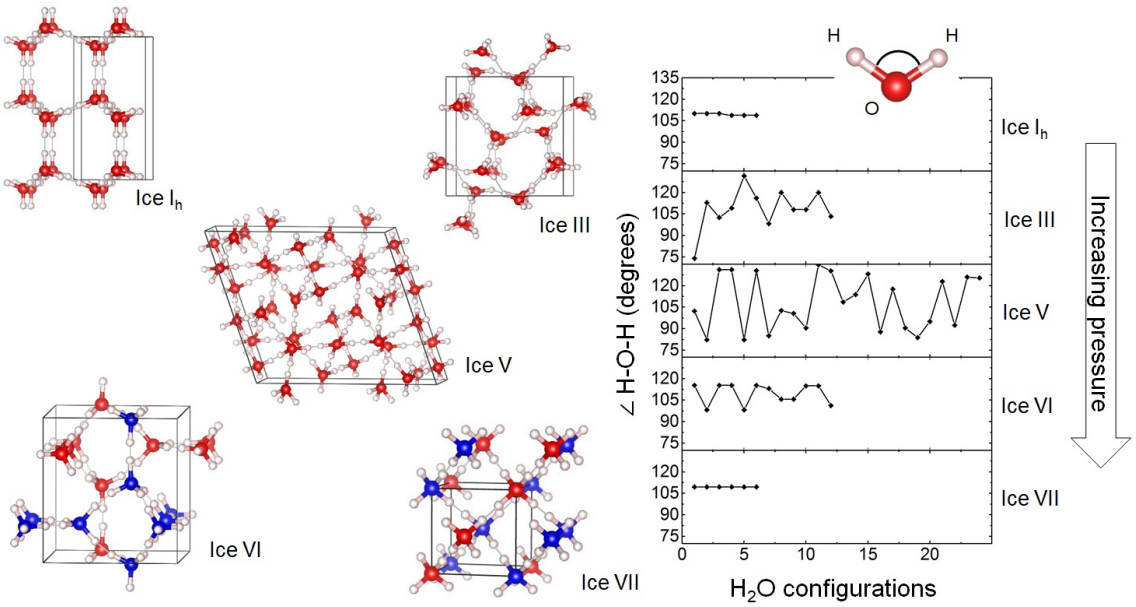

FIG. 1.2: Several crystal structures and H-O-H angle dispersion in their crystal structures. The H-O-H angle dispersion of each ice polymorphs is based on data of each crystal structure (ice Ih: [24], ice III: [25], ice V: [26], and ice VI and VII: [27]). In the crystal structures of ice VI and VII, two colored oxygen atoms represent two independent hydrogen-bonded networks. Black square of each crystal structure shows its unit cell.

Whalley (1966) reported hypothetical energy differences between ice Ih and other high-pressure phases at ambient pressure (see Fig. 1.3 and [28]). As shown in the figure, the structures of disordered phases energetically degenerate comparing with the room-temperate energy scale (26 meV at 300 K) up to ice VI. In other words, pressure potentially controls such energy differences, about 20 meV, beyond activation energies with reforming of oxygen frameworks. This is an important implication for this thesis. Actually such energy degeneracy is also reported among hydrogen-ordered configurations in disordered phases including ice VI focused on in this thesis (e.g. [29–31]). Ice VI and its hydrogen ordered phase, ice XV, are in a wide pressure region from 1 to 2 GPa. From its wide pressure range, there is a possibility that some stable hydrogen-ordered phases exist corresponding to ice VI in addition to ice XV [31]; the expectation is confirmed in this study.

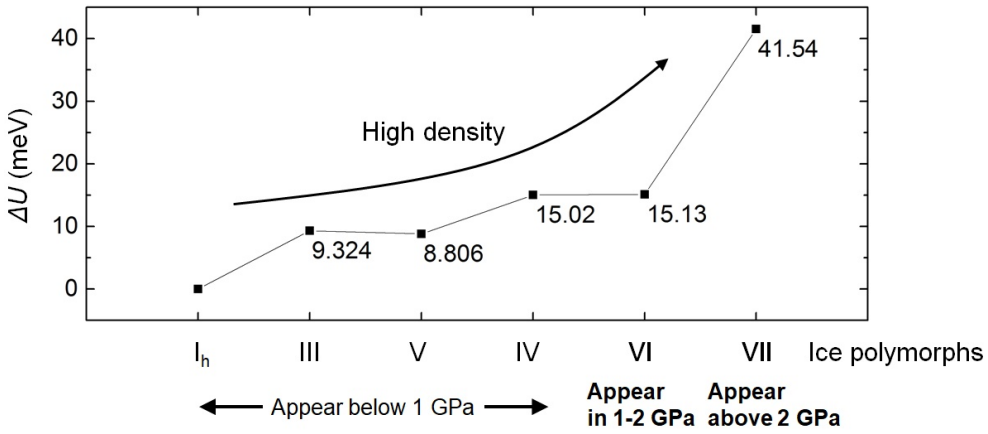

FIG. 1.3: Hypothetical energy differences between ice Ih and other high-pressure disordered phases at ambient pressure. Ice polymorphs are displayed in order of their density. This figure was made based on previous study reported in [28].

1.3 Discovery of hydrogen ordering from ice Ih

As mentioned in the above section, hydrogen ordering is one of the biggest reasons for the diversity of ice polymorphs in addition to the geometrical features. It is meaningful for this study to historically review the discovery of ice XI, which is an ordered phase of ice Ih. Because its discovery history includes the essential theme of my thesis, such as ice rule and point defects in ice. Before starting this section, we confirm the ice rule [15] as follows. 1) An oxygen atom has two covalent and two hydrogen bonds with four hydrogen atoms, respectively. 2) Two hydrogen atoms cannot simultaneously occupy their sites between hydrogen-bonded oxygen atoms. The first rule means that water molecules keep their molecular structures even in their solid state, ice. The second one constraints water molecule alignment considering electrostatic repulsion between hydrogen atoms.

1.3.1 Disordered states of ice Ih

In hydrogen-disordered and ordered states of ice, hydrogen atoms take 50 and 100% occupancy on their sites in time and space average. In a disordered state, water molecules have random orientations and change their directions through molecular rotation and proton translation dynamics by thermal fluctuation. In lower temperature, the thermal fluctuation is suppressed with the dynamics. This suppression is represented in the TS term of Gibbs free energy expression: $G = H - TS$. Additionally, it is expected from this equation that the most stable ordered phase

appears among possible hydrogen-ordered configurations obeying ice rule. Based on this expectation, hydrogen ordering of ice Ih had been investigated, though no study had reported about the hydrogen ordering for a long time. Especially from calorimetry study of ice Ih, non-zero entropy was reported at 0 K by Giauque and Stout (1936) (the residual entropy was estimated as 3.43 (J/K·mol) at 0 K from extrapolation of measured data in 15-273 K temperature region [32]). From this result, it was clarified that configuratinal entropy of the disordered state of ice Ih is remained at 0 K contrary to the third law of thermodynamics, so-called residual entropy problem (the problem has been considered as non-equilibrium process toward hydrogen-ordering).

1.3.2 Pauling's statistical model

For the residual entropy, Pauling (1935) gave micro-scale interpretation of its derivation considering combinations of hydrogen-ordered configurations [33]. We consider an ideal system composed of a large number of water molecules, represented N. Additionally, we assume that the ideal system is under 0 K temperature condition; this means configurational entropy only contributes to all entropy without such as atomic or molecular dynamical entropy. There are $2N$ sites of hydrogen atoms between hydrogen-bonded oxygen atoms, and so that the numbers of ordering ways are $4^N (= 2^{2N})$ ignoring the ice rule. Next, we consider hydrogen-ordered configurations surrounding a water molecule.

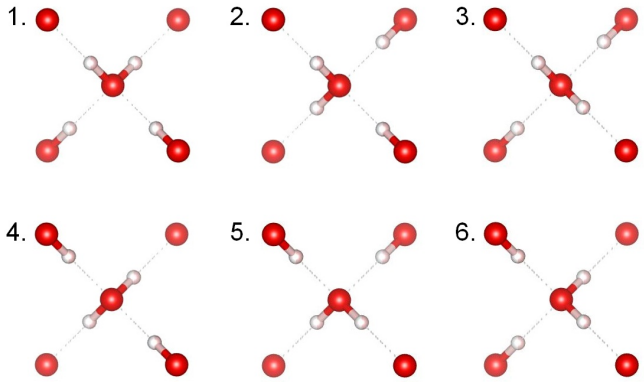

FIG. 1.4: Six configurations to keep ice rule for a water molecule surrounded by four water molecules.

As shown in Fig. 1.4, there are six configurations which obey ice rule. Then among all hydrogen-ordered configurational patterns, 4^N, it can be estimated that

there are $(3/2)^N (= 4^N \times (6/16)^N)$ possible hydrogen ordered configurations to obey ice rule. This is equivalent to numbers of states, and so that entropy at 0 K can be estimated as follows, $Nk_B \ln(3/2) = 3.37$ (J/K·mol), where N takes 1 mol and k_B is Boltzmann constant. This estimated entropy is well matched to the experimentally determined residual entropy. Now it is clarified that the almost all configurations form the disordered state of ice Ih. Additionally, the disordered state of ice Ih keeps its configurational entropy down to 0 K. But why hydrogen ordering does not occur?

1.3.3 Points defects

Debye (1929) pointed out that ice Ih is not a perfect crystal from its high dielectric constant, about 100 [34]. As shown in Fig. 1.5(a) if there is no defect in ice, water molecules should reorient their directions simultaneously to keep ice rule. Such an entire reorientation should have large activation energy. Based on this implication, it have been considered that the remaining of the disordered state of ice Ih is caused by the high activation energy toward hydrogen-ordered state under the limitation of ice rule.

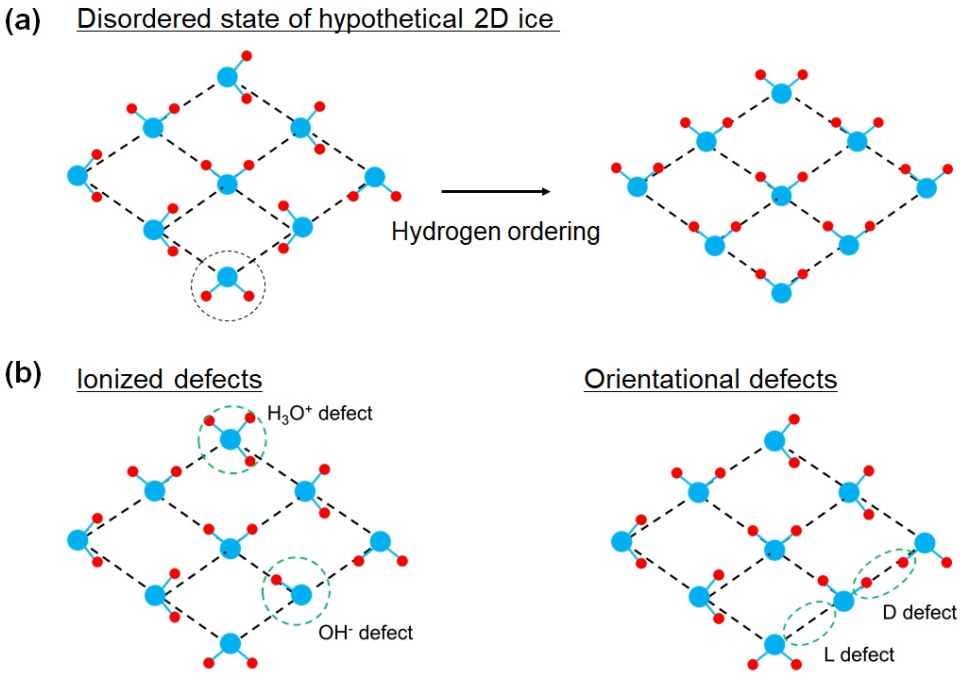

FIG. 1.5: (a) Schematic drawing of hydrogen ordering from disorder state of hypothetical 2D ice, which does not include defect. (b) Two types of point defects of ice, ionized and orientational defects.

About defects of ice, it has been considered that ice has two types of defects

related to a reorientation of water molecule, ionized and orientational defects (see Fig. 1.5(b) and [15]). Each defect includes (H_3O^+, OH^-) and (D, L) types, respectively (D, L is named from initial of doppelt and leer (corresponds double and empty in English) in Deutsch). With the ionized defects, water molecules change their direction through proton migration (translation). On the other hand, with the orientational defects, water molecules change their direction through molecular rotation. To artificially introduce these defects, many impurity-doping experiments were conducted. Most of them used alkali hydroxide, XOH (X = Na, K, Rb, Cs) and hydrogen halide HY (Y = F, Cl, Br, I) considering similarities of chemical compositions with H_2O. Kawada (1972) reported that hydrogen-ordered phase of ice Ih, ice XI, was induced by doping of KOH (concentration: 10^{-2} M) at 72 K from his dielectric measurements [19]. Furthermore, the hydrogen-ordered phase is the first reported ferroelectrically ordered phase of ice. In this thesis, a new hydrogen ordered phase of ice VI was found by using HCl dopant with concentration of 10^{-2} M . Dielectric measurements showed activated reorientations of water molecules. Additionally, I report that the two different dynamics, molecular rotation and proton translation, make different disordered states even in non-doped ice VII depending on pressure.

1.4 Principles of dielectric and neutron diffraction measurements

1.4.1 Dielectric measurement

In this study, dielectric measurements were mainly used to know how active the two dynamics are. Dielectric properties include mainly three physical values, dielectric constant (ϵ'), dielectric loss (ϵ'') and relaxation time (τ). Dielectric constant and loss are real and imaginary part of complex dielectric constant: $\epsilon^* = \epsilon' + i\epsilon''$. The complex dielectric constant is defined by $P = \epsilon^* E$, where E and P mean applied electric field and polarization induced by the electric field; in other words, dielectric constant represents a response of sample toward the applied electric field. These dielectric properties show frequency dispersion toward the applied electric field as the same as other physical values. Frequency dispersion of dielectric constant and loss can be introduced using micro scale atomic or molecular dynamics model and in ice case, they can be explained by Debye's model [15];

$$\epsilon'(\omega) - \epsilon_\infty = \frac{(\epsilon_s - \epsilon_\infty)}{1 + (\omega\tau)^2}, \quad \epsilon''(\omega) = \frac{(\epsilon_s - \epsilon_\infty)\omega\tau}{1 + (\omega\tau)^2}, \tag{1}$$

where $\omega = 2\pi f$ holds and f is frequency. Relaxation time, τ, is defined by $\tau = 1/2\pi f_0$ and f_0 is a frequency, where the dielectric loss becomes maximum. ϵ_s and ϵ_∞ represent low and high frequency limit of the dielectric constant, respectively. The left side of Fig. 1.6 shows a typical dielectric response obeying Debye's model. If AC electric field is applied to ice, for example, a water molecule tries to follow the applied electric field (its schematic drawing is shown in the right side of Fig. 1.6). As can be seen in the left side of Fig. 1.6, the AC frequency is enough slow for a water molecule to follow, ice shows large response in dielectric constant. In much higher AC frequency region, the water molecule cannot follow the frequency and the response is weakened. Dielectric loss has a peak at the changing region of dielectric constant. Dielectric relaxation corresponds the inverse frequency of the peak center of dielectric loss.

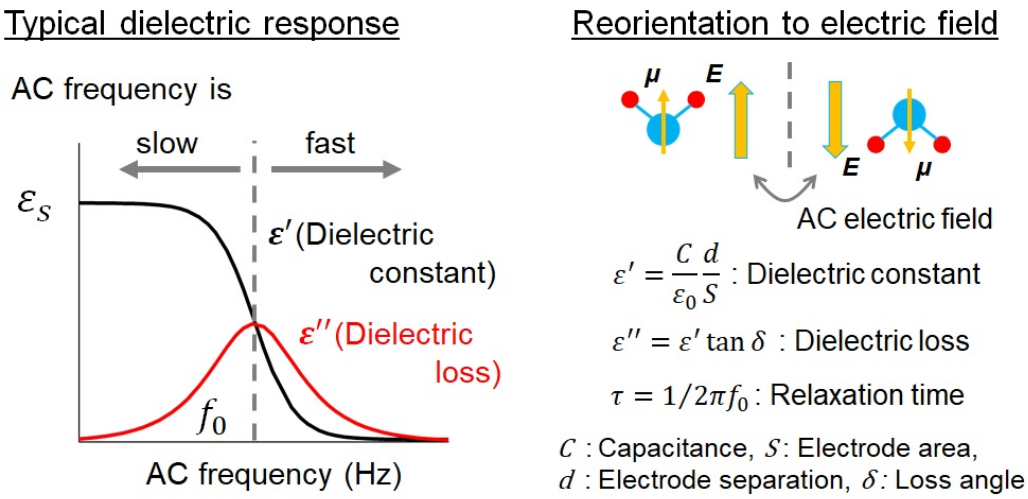

FIG. 1.6: Typical dielectric response obeying Debye's model (left side) and schematic drawing of the response of water molecule toward applied electric field (right side). The lower-right equations represent principle equation of dielectric constant, loss and relaxation time from obtained data.

From the equation (1), we can find a relationship between dielectric constant and loss, so-called Cole-Cole plot;

$$[\epsilon'(\omega) - \frac{\epsilon_s + \epsilon_\infty}{2}]^2 + \epsilon''(\omega)^2 = [\frac{(\epsilon_s - \epsilon_\infty)}{2}]^2, \quad \text{where } \epsilon''(\omega) \geq 0. \tag{2}$$

Though Cole-Cole plot can be drawn by semi-circle as shown in the equation, there are few cases that dielectric samples show the semi-circle response. In most samples, a semi-circle center shifts to -$|\epsilon''(\omega)|$ region; this corresponds a peak broadening of dielectric loss and physically means its dielectric relaxation time has a distribution

in the sample due to spatial inhomogeneity. This distribution can be represented by the following equation using a distribution parameter α;

$$\begin{aligned}\epsilon' - \epsilon_\infty &= \frac{(\epsilon_s - \epsilon_\infty)[1 + (\omega\tau)^{1-\alpha}\sin(\alpha\pi/2)]}{1 + 2(\omega\tau)^{1-\alpha}\sin(\alpha\pi/2) + (\omega\tau)^{2(1-\alpha)}}, \\ \epsilon'' &= \frac{(\epsilon_s - \epsilon_\infty)[(\omega\tau)^{1-\alpha}\cos(\alpha\pi/2)]}{1 + 2(\omega\tau)^{1-\alpha}\sin(\alpha\pi/2) + (\omega\tau)^{2(1-\alpha)}},\end{aligned} \tag{3}$$

where $0 < \alpha \leq 1$, and when $\alpha = 0$ holds the representation is equivalent to the single dispersion case. In this thesis, I used these equations, (3), for data fit of dielectric properties of ice. Finally, it should be noted that there is difference between dielectric responses derived from the molecular rotation and proton translation dynamics in terms of their pressure dependence. In the case of molecular rotation, the dynamics has a positive activation volume and so that the dynamics slow down with increasing pressure. On the other hand in proton translation case, an activation energy of the dynamics, which corresponds potential barrier between hydrogen-bonded oxygen atoms, goes down with increasing pressure because of the shortening of the O-O interatomic distance. Hence, the proton translation dynamics is activated under compression, and each dielectric response shows opposed frequency shift with increasing pressure. Owing to this, it is capable to distinguish which dynamics causes an observed dielectric response.

1.4.2 Neutron diffraction measurement

Neutron diffraction measurement was employed to determine positions of hydrogen atoms of ice. Neutron is scattered by nucleus, and this scattering makes a notable feature of neutron experiments; low electron density atoms are observable in neutron experiments unlike X-ray experiments. The scattering can be classified into elastic and inelastic scattering in terms of energy conservation. In diffraction measurement, we hypotheses elastic scattering to estimate diffraction patterns from samples. For neutron diffraction study, two types of neutron sources generally used; one is monochromatized neutron beam and the other one is pulsed white neutron beam. In each neutron source, diffraction experiments are conducted by angle and energy dispersive methods based on Bragg's formula, $n\lambda = 2dsin\theta$. In energy dispersive diffraction experiments, time of flight (TOF) method is usually used. Pulsed white neutron beam comes from neutron source with a energy dispersion and neutrons reach a sample at different times depending on their velocity. The velocity can be calculated as follows, $v = t/L$ (t: arrival time, L: flight length). From de

Broglie's relationship, $mv = h\lambda$, we obtain $\lambda = ht/mL$. Then using Bragg's formula, final representation for lattice spacing, d, is written as follows:

$$d = ht/2mLsin\theta. \tag{4}$$

Figure 1.7 shows schematic drawings of angle and energy dispersive type diffraction measurements. The new hydrogen ordered study of ice VI was conducted by energy dispersive type setting at high-pressure neutron beamline PLANET, J-PARC. Neutron diffraction experiments in this thesis were conducted using deuterated samples considering incoherent scattering of hydrogen atom. Generally scattering can be also classified into coherent and incoherent scattering. They respectively contribute Bragg reflection and background noise. It is known that hydrogen atom has a large incoherent component and deuterated samples are often used especially in the case of powder diffraction experiments. Because Bragg peaks are relatively smaller than that from single crystal samples.

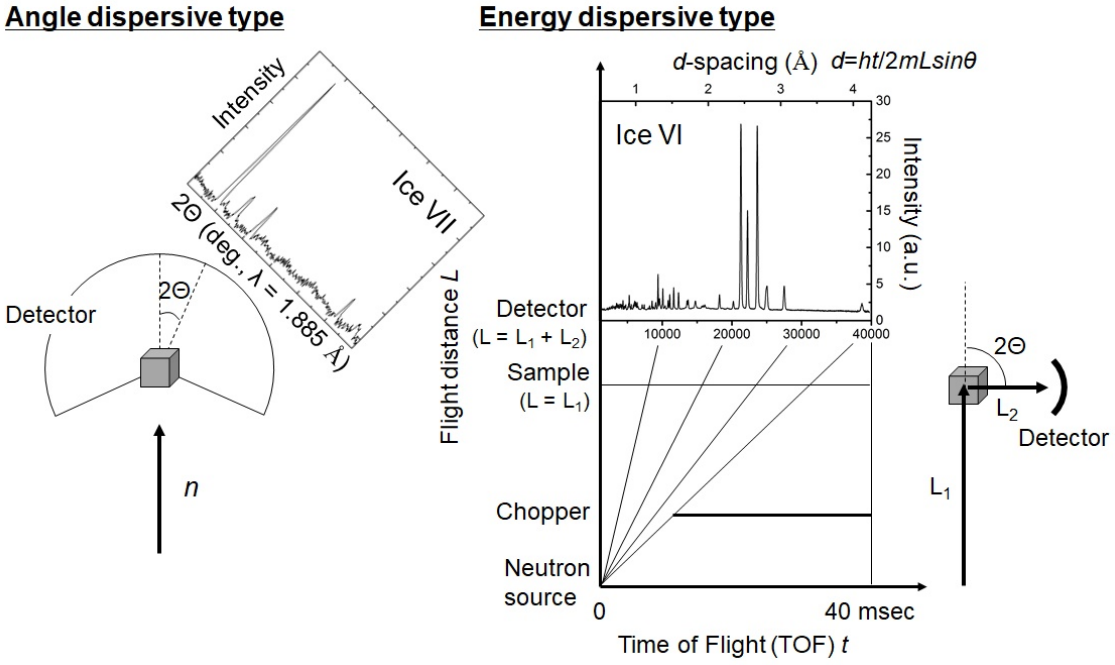

FIG. 1.7: Schematic drawings of two types of neutron scattering measurements, angle and energy dispersive type, shown in the left and right side. The schematic drawing of energy dispersive type is drawn based on high-pressure neutron beamline PLANET at J-PARC.

1.5 Objective and contents of this thesis

This thesis is based on phase studies of ice from the viewpoint of hydrogen disorder-order phase relationship and proton dynamics. About the former theme, this study is motivated to find new hydrogen ordered phases. In light of the most notable feature of ice, diversity of its polymorphs, discoveries of new ice polymorphs have been always main subject of ice. Historically, the discoveries have been achieved by unique experimental techniques and procedures. This study, on the other hand, is aimed to find out new phase relationship between disordered and ordered phases rather than to develop a technical breakthrough; up to now, one-to-one correspondence has been known in a pair of disorder and order phase [1]. However, considering energy degeneracy among possible hydrogen configurations, there is a possibility that one-to-many correspondence is found for one disordered phase. I especially focused on a case where appearance of ferroelectrically ordered structure (abbreviated FE ordered structure hereafter) is theoretically predicted in addition to known ordered phase having antiferroelectrically ordered structure (abbreviated AFE ordered structure hereafter). If the FE ordered structure is found experimentally, the discovery will contribute in the knowledge of how orientations of water molecules affect ice structure, stability, and other physical properties comparing with AFE ordered structure. On the other hand, the objective of proton dynamics study is to conduct first experimental direct observation of the dynamics. To my knowledge, the existence of proton dynamics has not been experimentally observed yet, although that is theoretically confirmed. Considering that the idea of proton dynamics, so-called Grotthuss mechanism, have been extensively accepted in other hydrogen materials, it is clearly important to obtain experimental evidence in ice. As mentioned before, a notable feature of the dynamics is that it is activated with increasing pressure in contrast to the molecular-rotation dynamics. So that high-pressure ice is the best field to valid the idea. For these purposes, I studied two unresolved problems related to disordered high-pressure phases, ice VI and VII, respectively. About ice VI, an existence of unknown hydrogen-ordered phase is experimentally suggested besides known AFE ordered phase, ice XV (e.g. [35]). Taking account of other theoretical reports into consideration (e.g. [31]), there is a possibility that the unknown ordered phase has a FE ordered structure. In ice VII, on the other hand, anomalous behavior has been reported at around 10 GPa (e.g. [36]). The anomalous behavior is interpreted in two scenarios; one is about dominant dynamics change of disordered

state of ice VII between molecular rotation and proton translation (e.g. [37]), and the other one is about partial coexistence of FE and AFE ordered domain in ice VII [38]. To clarify the unresolved problems, this thesis consists of four chapters from 2 to 5.

In Chapter **2**, the possibility of existence of new hydrogen-ordered phase of ice VI was verified by high-pressure dielectric and neutron diffraction experiments. Ice VI appears from 1 to 2 GPa pressure region, and dielectric experiments were comprehensively conducted in the wide pressure region. The existence of a new ordered phase was actually clarified in the dielectric experiments. Based on a new phase diagram obtained in the dielectric experiments, neutron diffraction measurements were conducted to determine a crystal structure of the new phase at 1.6 and 2.2 GPa, where the new phase is stable instead of the known AFE ordered phase of ice VI, ice XV.

In Chapter **3**, the anomalous behavior of ice VII at around 10 GPa was investigated according to the scenario about dominant dynamics change of disordered state of ice VII from molecular rotation to proton translation. Taking account of expected time scale of the two dynamics, mHz–MHz [39], dielectric experiments were conducted in ice VII beyond 10 GPa using a newly developed high-pressure cell.

In Chapter **4**, the possibility of partial coexistence of FE and AFE ordered domain in ice VII is verified as an interpretation of the anomalous behavior of ice VII. The AFE ordered structure corresponds to hydrogen-ordered phase of ice VII, ice VIII. In this study, the unknown FE ordered structure is especially focused. Theoretical previous studies reported that the FE ordered domains grow under high electric field [38]. Considering this theoretical prediction, high electric-fields (up to 10 kV/mm) was also applied in addition to high-pressure to find the FE ordered form by neutron diffraction measurements. This neutron diffraction experiment under high-electric fields and high pressure is original technique itself, and instrumental developments about the technique are also described in this chapter.

In Chapter **5**, technical developments of high-pressure dielectric measurements are described separately from experimental results corresponding to chapter 2 and 3. Two different cell assemblies were developed in this study using piston-cylinder and Bridgman-anvil type high-pressure apparatuses, respectively. They were used depending on target pressures in chapter 2 and 3.

第二章については、5 年以内に雑誌等で刊行予定のため、非公開。

第三章については、5 年以内に雑誌等で刊行予定のため、非公開。

4 Search for a ferroelectrically ordered form of ice VII by newly developed neutron diffraction under high pressure and high electric field

4.1 Introduction

In the previous chapter, it was clarified that the anomalous behavior of ice VII at around 10 GPa is caused by dominant dynamics crossover of ice VII. The structural anomaly, reported as a peak splitting (or broadening) in X-ray diffraction pattern, is interpreted as relatively hydrogen-ordered state of ice VII in the dynamics crossover. Because the peak splitting generally means symmetry lowering of samples. Somayazulu et al. (2008) suggested a possibility that a pressure-induced partial hydrogen ordering occurs at around 10-15 GPa [63]. The ordered phase of ice VII is ice VIII, which has an antiferroelectrically ordered structure (called "AFE structure" hereafter, and its crystal structure is shown in Fig. 4.1, space group $I4_1/amd$). The AFE structure has been considered as a candidate for the partially ordered structure in ice VII (if ice VII is really partially ordered). However, Caracas and Hemley have proposed a different scheme for the partial ordering of ice VII by using density functional theory calculations [38]. They proposed that a ferro-electrically ordered structure (called "FE structure" hereafter, and its crystal structure is shown in Fig. 4.1, space group $P4_2nm$) could occur in ice VII at a bulk scale under high-electric field. Their calculations show that the AFE structure is slightly more stable than the FE structure, but the energy difference between AFE and FE structures was so small ($\sim$10 meV/molecule) that the FE structure could be stabilized under an external electric field. Their calculation also shows that the energy difference slightly decreases from 12.3 meV/molecule at 2 GPa to 11.7 meV/molecule at 10 GPa with increasing pressure. The energy difference between FE and AFE is almost comparable below 10 GPa; it will be predicted, from the estimated volume fraction of the FE structure at pressure lower than 10 GPa, how much the ferroelectrical ordering is induced by high electric field in ice VII above 10 GPa. In this study, high-pressure and high electric-field neutron experiments were conducted at up to 6.2 GPa with overcoming some technical difficulties as mentioned later.

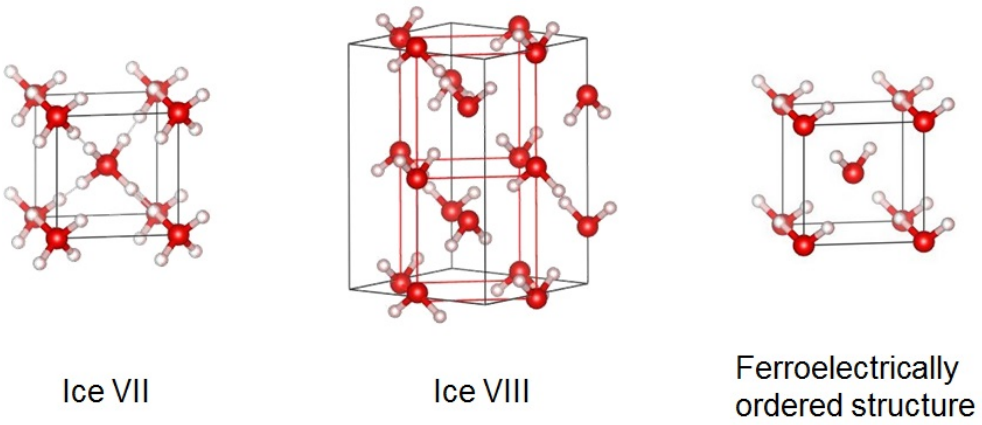

FIG. 4.1: Crystal structures of ice VII, ice VIII, and hypothetical ice with ferroelectrically ordered structure (FE structure). The black lines show the unit cells and the red line in ice VIII corresponds to the unit cell of ice VII.

If the FE structure is found experimentally, the discovery will contribute not only for the understanding of the anomalies observed in ice VII but also in the knowledge of how orientations of water molecules affect ice structure, stability, and other physical properties.

Neutron diffraction experiments under high pressure and high electric field would be the most direct method to find the FE structure, however such measurements had previously been technically unfeasible. In general, cooperative phenomena among dipoles are induced by electric field in an order of kV/mm across samples of order tens to hundreds μm thickness as this enables a large electrical field to be generated with a limited voltage. This is rather incompatible with the thin samples required to achieve high pressures. Additionally, neutron diffraction requires larger volume samples, at least a few mm^3, to obtain sufficient diffraction intensity, because of the relatively weak nature of neutron sources. A further difficulty is that the electrodes to apply a high electric field have to be electrically insulated, challenging in the close confines of a high-pressure cell.

I recently overcame these technical difficulties and developed a cell assembly for *in situ* neutron diffraction experiments under high-pressure and high electric fields, and here I present neutron diffraction patterns of ice VII at room temperature, at pressures up to 6.2 GPa and at electric field up to 10.2 kV/mm.

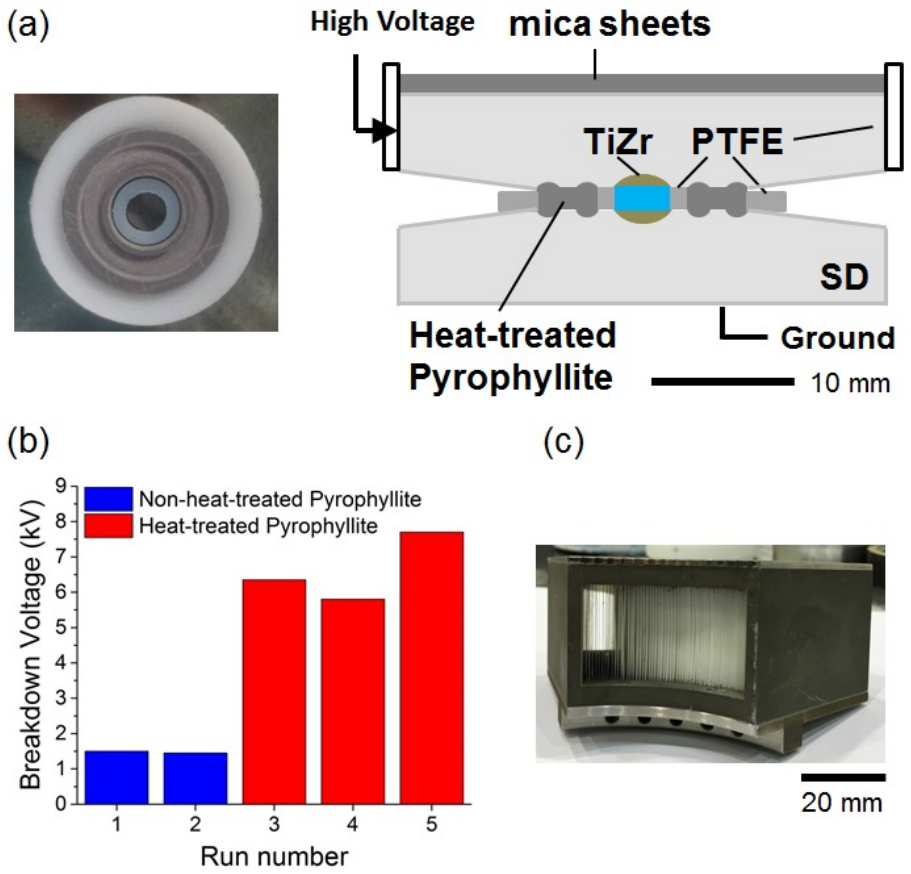

FIG. 4.2: (a) Schematic drawings of cross section for a developed double-toroidal-type anvil cell assembly (right) and the picture of gaskets (left), where SD and PTFE denote sintered diamond and polytetrafluoroethylene, respectively. Samples, with a volume ∼20 mm^3, are loaded into the gaskets sandwiched by anvils, and compressed using a Paris-Edinburgh press (type VX5). The upper anvil was electrically connected to a high-voltage power supply, and was insulated from the press by using the PTFE collar and mica sheets. The bottom anvil was electrically grounded. (b) Breakdown voltages of the five experimental runs, by using non-heat-treated pyrophyllite (blue) and heat-treated pyrophyllite (red). (c) A picture of radial collimator developed for the Paris-Edinburgh press. Each partition of the radial collimator is made of Gd_2O_3-painted thin film. This was used to reduce the measured scattering contribution from the cell assembly.

4.2 Experimental methods

A picture and schematic drawings of the developed cell assembly are shown in Fig. 4.2(a). Double-toroidal type anvils were used to generate high pressure. The anvils are made of sintered diamond (abbreviated "SD" in Fig. 4.2(a)) with a cobalt binder, which works as an electric conductor. A coupled pair of spherical caps of TiZr null scattering alloy attached to the anvils with silver paste were used as electrodes in order to reduce scattering from the anvils and also to make electrodes parallel. The upper side of the anvil was electrically insulated from a high-pressure press by using

a PTFE collar and mica sheets (see more details in [71]). Heat-treated pyrophyllite rings (700°C, 1 h) were used as gaskets, as it was found that non-heat-treated pyrophyllite gaskets caused electrical breakdown at around 1.5 kV/mm, probably due to the hydrous component (Fig. 4.2(b)). It is noted that the breakdown at 6–8 kV in runs 3–5 (Fig. 4.2(b)) might not have occurred in the gaskets but around the PTFE collar and mica sheets, as the corresponding burns were actually observed on the collar and sheets, particularly focused around the corner of anvils. Despite this, we believe that this assembly (using heat-treated pyrophyllite and PTFE gaskets) could be used for higher voltage but optimization of anvil profiles may be necessary to avoid the electric discharge around the corner of the anvils. The inner PTFE ring was used to seal the water sample under initial loading and the outer PTFE ring works to ensure uniform deformation of the heat-treated pyrophyllite gasket under compression.

Neutron diffraction experiments were carried out on the High Intensity Powder Diffraction instrument, WOMBAT, at the ANSTO. The wavelength of neutrons used was 1.885 Å. A small radial collimator (Fig. 4.2(c)), having partitions made of Gd_2O_3 painted thin film, was set on the Paris-Edinburgh press to reduce the parasitic scattering from the high-pressure cell. Deuterated water (99.9%, Wako) was used as a sample and compressed at room temperature. Pressure was estimated from the observed unit cell volume of ice VII using the third-order Birch equation [61]. High voltage was applied to the electrically insulated upper side of the anvil using a high-voltage power supply (Matsusada AU-10R120). An electrode separation was measured in a separate run using a laser displacement sensor (KEYENCE, IG-028) (black square in Fig. 4.3). The reproducibility of sample pressure to the applied load in both the neutron and the additional experiments was confirmed by water $\rightarrow$ ice VI phase transition observed by *in situ* dc resistivity measurements of the samples (red triangle in Fig. 4.3).

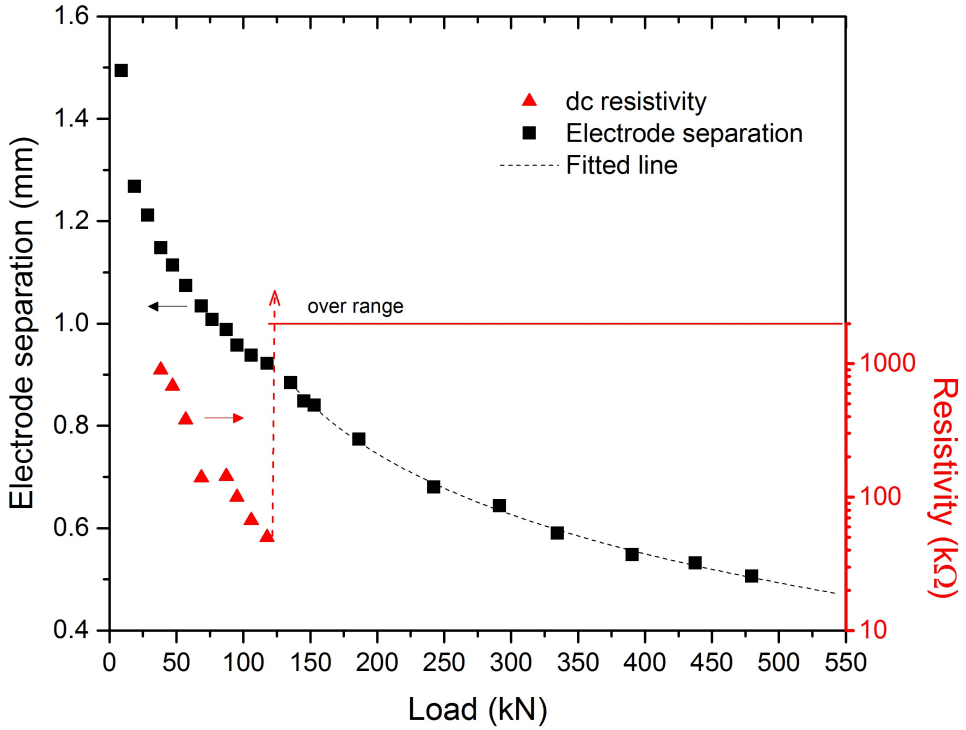

FIG. 4.3: Electrode separation (black square) and dc resistivity (red triangle) at respective loads. The electrode separation was estimated from anvil gap and the dc resistivity between two anvils was measured using an Iso-Tech IDM73 multimeter. The water → ice VI phase transition was observed in both measurements at around 130 kN. The dotted line is a polynomial fit to electrode-separation data above 130 kN.

Experimental conditions, pressure, applied voltage, and electrode separation are listed in Table 4.

Table 4: Pressure, applied voltage, and electrode separation conditions.

Pressure (GPa)	Voltage (kV)	Electrode separation (mm)
3.2	1.5, 2.0, 2.5, 3.0, 3.5, 4.0, 4.5, 5.0	0.68
4.9	2.0, 3.0, 4.0, 5.0	0.57
6.2	2.0, 3.0, 4.0, 5.0	0.49

4.3 Results and Discussion

Figure 4.4 shows neutron diffraction patterns at 6.2 GPa, the highest pressure I obtained, with applying electric fields up to 10.2 kV/mm. All visible peaks in the diffraction patterns can be indexed as 110, 111, and 211 reflections of ice VII, or 110

of diamond (anvils). The FE structure would give two peaks at around 70° and 80° 2θ as discussed later. As it can be seen, these additional peaks were not observed in the diffraction patterns at any pressure and electric-field conditions.

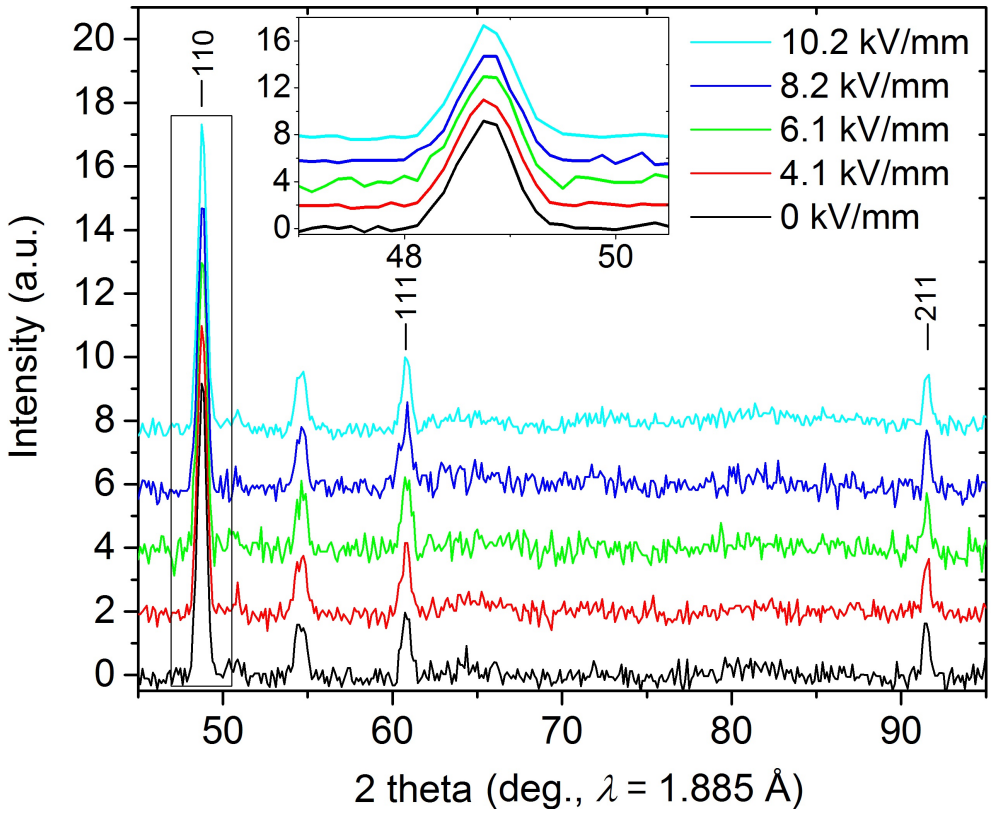

FIG. 4.4: Neutron diffraction patterns at 6.2 GPa and with electric fields of 0, 4.1, 6.1, 8.2, and 10.2 kV/mm. Exposure times were 1, 1, 0.5, 0.5, and 2 h, respectively. These conditions of electric field are estimated from the applied voltage and the electrode separation at respective pressures from the line drawn in Fig. 4.4. The inset shows expanded plots at around 50°. From lower angle, 110, 111, and 211 reflections of ice VII are observed. The peak at around 55° is 110 reflection of diamond (anvils). The undulation from 60° to 90° could be derived from inhomogeneous gaps of the radial-collimator partitions.

I note that the noise level of the observed diffraction patterns are comparable to the Bragg peaks, although the developed radial collimator significantly reduced the parasitic scattering from the cell. It is still possible that the peaks derived from the FE structure may be hidden under the noise level. Consequently, to discriminate this, we simulated how the FE structure could be observed in neutron diffraction patterns. If the FE structure is locally formed in ice VII, the ordered region would increase with increasing electric field. This partially ordered state could be described by a mixed phase model of completely disordered ice VII and completely ordered

FE structure. In this model, the FE structure coexists as a domain structure with ice VII.

The mixed phase model of ice VII and the FE structure was simulated at a number of volume fractions (f) of the FE phase using GSAS [57] with EXPGUI [58] (Fig. 4.5). From this, we could estimate that, considering the noise level of the diffraction pattern, the volume fraction of the FE structure should be less than 0.10 if it was present in the 6.2 GPa and 10.2 kV/mm sample. The intensity of the 210 reflection in the case of $f = 0.10$ should be 1.5 times higher than the averaged noise level, hence this reflection should be visible if f is larger than 0.10.

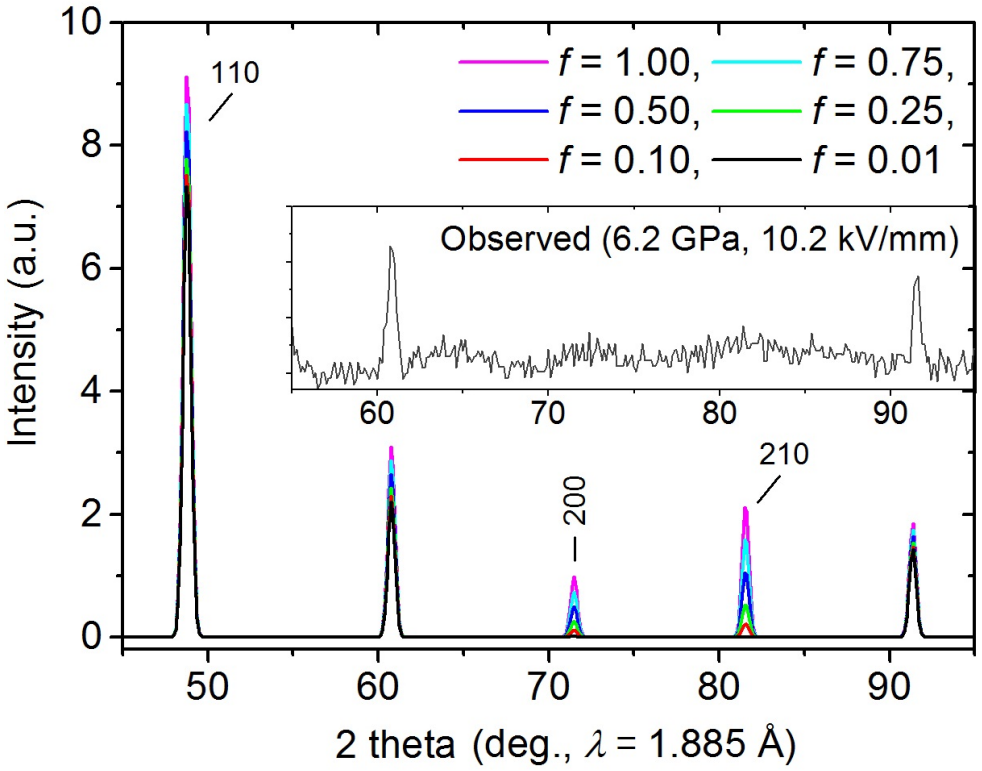

FIG. 4.5: Simulated neutron diffraction patterns of the mixed phase of ice VII and completely ordered FE structure (space group: $Pn\bar{3}m$ and $P4_2nm$). f represents a volume fraction of FE structure. Inset shows the observed diffraction pattern at 6.2 GPa and 10.2 kV/mm at around 60°–90°. 200 and 210 peaks appear with increasing the volume fraction of FE structure.

The volume fraction of the FE structure can also be estimated from electric-field-induced polarization. When an electric field is applied to ice VII, electric polarization, related to the volume fraction, increases corresponding to the dielectric constant of ice VII and the strength of the electric field. This polarization causes experimentally observable induced charge on electrodes attached to ice VII. Here-

after I introduce approximate relationship between the volume fraction and electric polarization in ice VII and estimate the volume fraction in light of measurements of electric polarization, which is more sensitive to increases of the volume fraction.

Electric polarization ($\mathbf{P}$) is found by a summation of dipole moments in a unit volume: $\mathbf{P} = \sum_i \boldsymbol{\mu}_i$, where i is an index of a water molecule, and $\boldsymbol{\mu}_i$ means a dipole moment of i-th water molecule. In the case of ice VII, which possesses center symmetry, the summation of $\boldsymbol{\mu}_i$ is canceled out by disordered orientation of water molecules under zero electric field. If the orientation of the electric field is defined as the z axis, $P = |\mathbf{P}| = \sum_i (\mu_z)_i$ holds, where $(\mu_z)_i$ means a z component of $\boldsymbol{\mu}_i$. Hereafter $|\boldsymbol{\mu}_i|$ is considered as $\mu\,(= 6 \times 10^{-22}\,\mu\mathrm{C} \cdot \mathrm{cm})$, the strength of a dipole moment of a water molecule in a gas phase at room temperature and ambient pressure, for any i-th water molecule. In order to derive the volume fraction of the FE structure from the polarization, we assumed that the polarization P is all contributed from completely oriented water molecules of the FE structure along electric field,

$$P = \mu N_p, \tag{8}$$

where N_p is a hypothetical number density of the completely oriented water molecules. Additionally, let $N\,(= 6 \times 10^{22}\,/\mathrm{cm}^3)$ be a number density of water molecules in ice VII, which can be calculated using the equation of state of ice VII [61], and then N_p/N can be considered to be equal to the volume fraction. We obtain a relationship between the volume fraction and electric polarization;

$$f = P/\mu N. \tag{9}$$

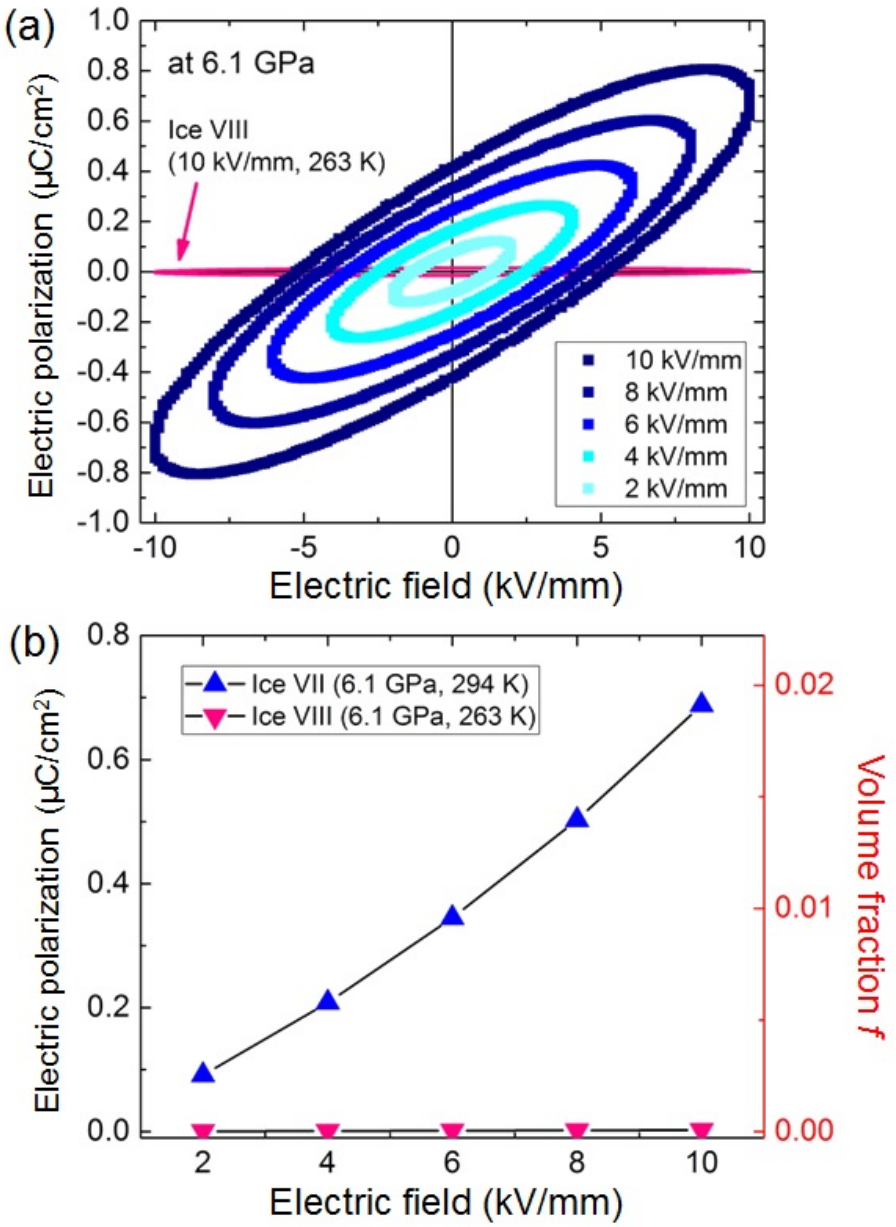

FIG. 4.6: (a) *P-E* loops at 6.1 GPa with 2, 4, 6, 8, and 10 kV/mm ac electric field. The pink loop corresponds to ice VIII at 263 K with 10 kV/mm. Temperature was measured by *K*-type thermocouple attached to the surface of opposed anvils. (b) Electric-field dependence of electric polarization and the calculated volume fraction using Eq. (2). Electric polarization under 2, 4, 6, 8, and 10 kV/mm is shown at each applied ac electric fields.

Electric polarization was measured at high pressure by using a different cell assembly, improved from our previous development using hole-type opposed anvils (see [7] and the Supporting information of this chapter for a detailed description of the cell assembly for our electric polarization measurements under high pressure).

A notable feature of this cell is that only the sample is sandwiched by electrodes, and this feature allows us to measure induced charge on the electrodes derived from the sample. Electric polarization was observed by *P*-*E* loop methods using an op-amp-type Sawyer-Tower circuit with 50 Hz ac high voltage. The results of the *P*-*E* loop measurements at 6.1 GPa with ac electric fields, 2, 4, 6, 8, and 10 kV/mm, are shown in Fig. 4.6(a). Ice VIII data at 263 K with 10 kV/mm is also shown for comparison to electric polarization of ice VII. Typical paraelectric behavior was observed in ice VII; the observed electric polarization was induced by electric field linearly, though our data show as ellipsoid due to a contribution from the electric conductive component of ice VII. In ice VIII, on the other hand, electric polarization was not induced. This is consistent with the antiferroelectric-type crystal structure of ice VIII and a previous dielectric study of ice VIII reported by Whalley *et al.* [72]. Electric polarization of 2, 4, 6, 8, and 10 kV/mm at each ac electric field is shown in Fig. 4.6(b). The right axis shows the volume fraction calculated using Eq. (9) and the volume fraction is estimated as about $f = 0.02$ at 6.1 GPa with 10 kV/mm. It is noted that we conducted *P*-*E* loop measurements three times to confirm reproducibility and estimated volume fraction was in the range 0.01–0.02 among the three runs. In this order of the volume fraction, the expected reflections from the FE structure would be hidden in our neutron diffraction experiments. It should be noted that the polarization of the FE structure is not only oriented along the z axis, but also has different orientations, as the sample was polycrystalline. This means that actual contribution of the FE structures with different orientations to the polarization would be lower than the case of Eq. (8). In other words, a more locally formed FE structure should contribute to yield the polarization P and the calculated volume fraction by Eq. (9) would be underestimated. When higher electric fields are applied, for example 30 and 50 kV/mm, the f would increase 0.06 and 0.11 from linear extrapolation of the electric-field dependence of the volume fraction shown in Fig. 6(b). At 50 kV/mm, a peak height ratio (the strongest 110 reflection):(the 210 reflection) is 30:1, so that the 210 peak would be observable considering the signal/noise ratio.

4.4 Conclusion

In conclusion, I have carried out neutron diffraction experiments of ice VII under both high-pressure and high electric fields of up to 10.2 kV/mm. This was achieved by using the developed high-pressure cell assembly. No clear evidence of the appearance of the ferroelectrically ordered structure was obtained from the observed diffraction patterns. Simulations based on the mixed phase model show that the volume fraction of the FE structure should be less than 0.10, even in the case that the FE structure exists in ice VII and the peaks from the FE structure are hidden in the noise level. This constraint is consistent with the estimated volume fraction $f = 0.02$ from high-pressure P-E loop measurement. Although further improvements for background reduction of the neutron diffraction patterns and for more electrical insulation would be necessary to find the potentially existing FE structure, the developed technique opens the way to find interesting properties of ice polymorphs, such as the discovery of a para-ferroelectric type phase transition, which would have a potentially high impact for phase study of not only ice but also many other hydrogen-bonded crystal systems.

4.5 Supporting information

$P-E$ loop measurements were conducted in order to estimate the volume fraction from the polarization P, using a newly developed cell assembly using opposed-type anvils with a hole. In this cell assembly, electrodes are electrically connected only to samples and insulated from other parts of the assembly such as the anvils and gaskets. Schematic drawings of cross-section for the improved cell assembly are shown in Fig. 4.7(a) and (b). The anvil, made of tungsten carbide (Silver Alloy, SA160), was used to generate high pressure with the culet size of Φ OD: 7 mm, ID: 4 mm. The anvils and gaskets were insulated from high voltage applied to the upper Cu lead covered with a polyimide tube (FURUKAWA ELECTRIC, PIT-S; ID: 0.20 mm, thickness: 0.04 mm) as shown in Fig. 4.7(c). The applied pressure was estimated from ruby fluorescence measurement. A small ruby tip was introduced just behind the electrode and exposed from the incident 532 nm laser beam travel through a plastic fiber (Edmund Optics, Φ 0.25 mm), and the induced fluorescence was also traveled through the fiber to the detector (Ocean optics, USB2000+). High voltage was applied to a Cu electrode (upper: Φ1.5 mm, bottom Φ2.0 mm, thickness: 0.05 mm) attached on the sample, water. In this high-pressure cell, the electrode area was estimated by using the dielectric constant of water, 78.5 at 297 K, and the initial electrode separation (we assumed that the electrode area does not vary with pressure change). The electrode separation was estimated by the same method as explained in chapter 3.

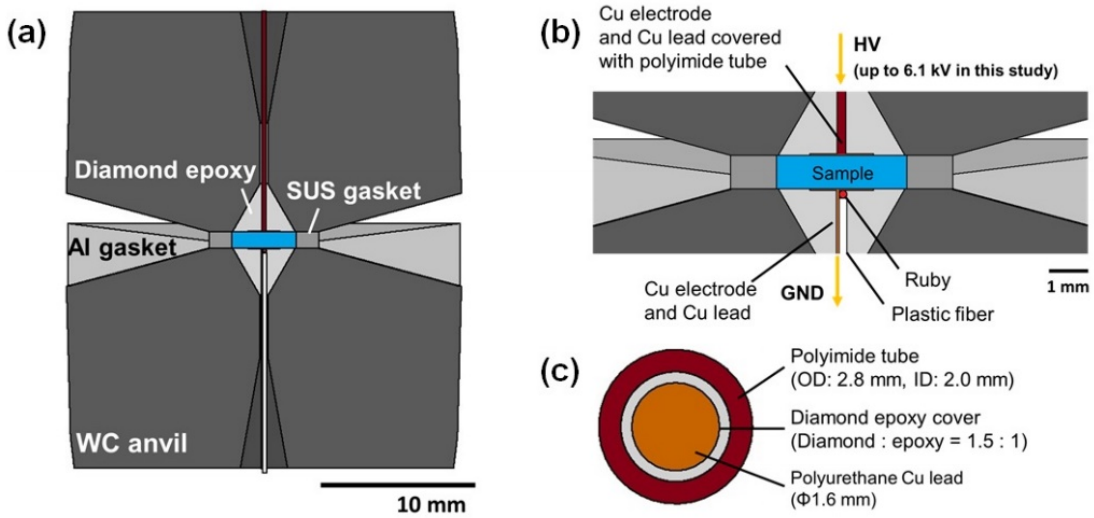

FIG. 4.7: (a) Schematic drawing of cross-section for a newly developed hole type anvil cell assembly. WC and diamond epoxy means tungsten carbide and mixture of diamond powder (Tomei Diamond, particle size: 1.0 μm) and epoxy resin (STYCAST® 1266 A/B): mass ratio = 3.8 : 1. Sample, with a volume $\sim$13 mm^3 is loaded into the gaskets sandwiched by anvils, and compressed using Paris-Edinburgh press (type-V4). (b) Schematic drawing of cell assembly around sample. High voltage (HV) of 6.1 kV was applied to the cell in most of our experiments. The upper Cu lead covered with polyimide tube is electrically connected to a high-voltage power supply (TEXIO, STW-9803) and insulated from the gaskets and anvils. (c) Schematic drawing of cross-section for the Cu lead covered with polyimide tube, where OD and ID mean outer and inner diameters, respectively.

第五章については、**5** 年以内に雑誌等で刊行予定の内容を含むため、非公開。

Appendix A, B については、**5** 年以内に雑誌等で刊行予定のため、非公開。

Acknowledgement

First of all I would like to express my deepest gratitude to Professor Kagi Hiroyuki and Associate Professor Kazuki Komatsu for their continuous educational, guidance, discussions, and encouragement.
I appreciate Mr. Shigemi Otsuka and Mr. Togo Shimozawa (Technical staff of University of Tokyo) for their significant contribution to my thesis. They helped me again and again by their very quickly and precise machining.
I am grateful to Dr. Taku Okada for accessing the impedance analyzer used in this study and to Prof. Takehiko Yagi, Dr. Katsutoshi Aoki,and Dr. Riko Oku-Iizuka for their advices for modifications of high pressure cell assembly especially about the Bridgman type high-pressure cell.
I wish to express thanks to Dr. Helen E. Maynard-Casely, Dr. Norman Booth and Mr. Stan Lee for their helpful assistance for neutron experiments at ANSTO. I am also grateful to all technical staff at ANSTO for their support to the experiments.
I am grateful to Professor Yoshiya Uwatoko, Assistant Professor Jun Gouchi and Research Associate Staff Shoko Nagasaki for their helpful technical advice for modifications of high pressure cell assembly especially about the Piston-cylinder type high-pressure cell. And also I appreciate Dr. Takanori Hattori (JAEA) and Dr. Shinichi Machida (CROSS) for their devoted technical support to my neutron experiments conducted at J-PARC (the neutron experiment at the Materials and Life Science Experimental Facility of the J-PARC was performed under a user program: Proposal No. 2019A0310).
I appreciate Mr. Ito for his contribution to the dielectric experiments in Chapter 2. Data of dielectric properties of non-doped ice VI were mainly measured by him as a part of graduation research. A further discussion of the data, especially about pressure dependence of the dielectric properties of non-doped ice VI will be described in his graduation thesis.
I also appreciate Ms. Chikako Fujimoto, Mr. Ko Fukuyama, Mr. Keishiro Yamashita for their continuous discussions and encouragement. I thank all my ex-colleagues in Kagi and Hirata group.
Finally, I would also like to express my deepest gratitude to my mother. Through my very long student life she always supported and encouraged me.
This thesis was financially supported by Grant-in-Aid for JSPS fellows for Young Scientists (DC2), Grant No. 18J13298.

References

1. Salzmann, C. G., Radaelli, P. G., Slater, B. & Finney, J. L. The polymorphism of ice: Five unresolved questions. *Physical Chemistry Chemical Physics* **13,** 18468–18480. ISSN: 14639076 (2011).
2. Arakawa, M., Kagi, H., Fernandez-Baca, J. A., Chakoumakos, B. C. & Fukazawa, H. The existence of memory effect on hydrogen ordering in ice: The effect makes ice attractive. *Geophysical Research Letters* **38,** 3–7. ISSN: 00948276 (2011).
3. Yamane, R. *et al.* Search for a ferroelectrically ordered form of ice VII by neutron diffraction under high pressure and high electric field. *Physical Review B* **99,** 174201. ISSN: 24699969. `https://doi.org/10.1103/PhysRevB.99.174201` (2019).
4. Thoeny, A. V., Gasser, T. M. & Loerting, T. Distinguishing ice β-XV from deep glassy ice VI: Raman spectroscopy. *Physical Chemistry Chemical Physics* **21,** 15452–15462. ISSN: 14639076 (2019).
5. Wilson, G. J., Chan, R. K., Davidson, D. W. & Whalley, E. Dielectric properties of ices II, III, V, and VI. *The Journal of Chemical Physics* **43,** 2384–2391. ISSN: 00219606 (1965).
6. Johari, G. P. & Whalley, E. The dielectric relaxation time of ice V, its partial anti-ferroelectric ordering and the role of Bjerrum defects. *Journal of Chemical Physics* **115,** 3274–3280. ISSN: 00219606 (2001).
7. Yamane, R., Komatsu, K. & Kagi, H. Note: Development of a new Bridgman-type high pressure cell for accurate dielectric measurements. *Review of Scientific Instruments* **88,** 046104. ISSN: 10897623. `http://aip.scitation.org/doi/10.1063/1.4980154` (2017).
8. Hernandez, J. A. & Caracas, R. Proton dynamics and the phase diagram of dense water ice. *Journal of Chemical Physics* **148.** ISSN: 00219606 (2018).
9. Marx, D. Proton transfer 200 years after Von Grotthuss: Insights from ab initio simulations. *ChemPhysChem* **7,** 1849–1870. ISSN: 14394235 (2006).
10. Horike, S., Umeyama, D. & Kitagawa, S. Ion conductivity and transport by porous coordination polymers and metal-organic frameworks. *Accounts of Chemical Research* **46,** 2376–2384. ISSN: 00014842 (2013).
11. Luo, C., Fa, W., Zhou, J., Dong, J. & Zeng, X. C. Ferroelectric ordering in ice nanotubes confined in carbon nanotubes. *Nano Letters* **8,** 2607–2612. ISSN: 15306984 (2008).
12. Zhao, H. X. *et al.* Transition from one-dimensional water to ferroelectric ice within a supramolecular architecture. *Proceedings of the National Academy of Sciences of the United States of America* **108,** 3481–3486. ISSN: 00278424 (2011).
13. Kusoglu, A. & Weber, A. Z. New Insights into Perfluorinated Sulfonic-Acid Ionomers. *Chemical Reviews* **117,** 987–1104. ISSN: 15206890 (2017).
14. Bridgman, P. W. Water, in the liquid and five solid forms, under pressure. *Am. Acad. Arts Sci* **47,** 441–558 (1912).
15. Fletcher, N. H. *The chemical physics of ice* (Cambridge University Press, 1970).
16. Whalley, E. Dielectric Properties of Ice VII. Ice VIII: A New Phase of Ice. *The Journal of Chemical Physics* **45,** 3976. ISSN: 00219606. `http://link.aip.org/link/?JCP/45/3976/1&Agg=doi` (1966).

17. Aoki, K., Yamawaki, H., Sakashita, M. & Fujihisa, H. Infrared absorption study of the hydrogen-bond symmetrization in ice to 110 GPa. *Physical Review B - Condensed Matter and Materials Physics* **54,** 15673–15677. ISSN: 1550235X (1996).

18. Lobban, C., Finney, J. L. & Kuhs, W. F. The structure of a new phase of ice. *Nature* **391,** 268–270. ISSN: 00280836 (1998).

19. Kawada, S. Dielectric Dispersion and Phase Transition of KOH Doped Ice. *Journal of the Physical Society of Japan* **32,** 1442 (1972).

20. Salzmann, C. G., Radaelli, P. G., Hallbrucker, A., Mayer, E. & Finney, J. L. The Preparation and Structures of Hydrogen Ordered Phases. *Science (New York, N.Y.)* **311,** 1758–1761 (2006).

21. Falenty, A., Hansen, T. C. & Kuhs, W. F. Formation and properties of ice XVI obtained by emptying a type sII clathrate hydrate. *Nature* **516,** 231–233. ISSN: 14764687. `http://dx.doi.org/10.1038/nature14014` (2014).

22. Del Rosso, L., Celli, M. & Ulivi, L. New porous water ice metastable at atmospheric pressure obtained by emptying a hydrogen-filled ice. *Nature Communications* **7,** 1–7. ISSN: 20411723. `http://dx.doi.org/10.1038/ncomms13394` (2016).

23. Millot, M. *et al.* Nanosecond X-ray diffraction of shock-compressed superionic water ice. *Nature* **569,** 251–255. ISSN: 14764687. `http://dx.doi.org/10.1038/s41586-019-1114-6` (2019).

24. Goto, A., Hondoh, T. & Mae, S. The electron density distribution in ice Ih determined by single-crystal x-ray diffractometry. *The Journal of Chemical Physics* **93,** 1412–1417. ISSN: 00219606 (1990).

25. Kamb, B. & Datta, S. Crystal Structures of the High-Pressure Forms of Ice : Ice III. *Nature* **187,** 140–141 (1960).

26. Kamb, B. Y. B., Prakash, A. & Knobler, C. Structure of Ice V, 706–715 (1967).

27. Kuhs, W. F., Finney, J. L., Vettier, C. & Bliss, D. V. Structure and hydrogen ordering in ices VI, VII, and VIII by neutron powder diffraction. *The Journal of Chemical Physics* **81,** 3612–3623. ISSN: 00219606 (1984).

28. Whalley, E. Energies of the phases of ice at zero temperature and pressure. *The Journal of Chemical Physics* **81,** 4087–4092. ISSN: 00219606 (1984).

29. Raza, Z. *et al.* Proton ordering in cubic ice and hexagonal ice; A potential new ice phase - XIc. *Physical Chemistry Chemical Physics* **13,** 19788–19795. ISSN: 14639076 (2011).

30. Tribello, G. A., Slater, B. & Salzmann, C. G. A blind structure prediction of ice XIV. *Journal of the American Chemical Society* **128,** 12594–12595. ISSN: 00027863 (2006).

31. Komatsu, K. *et al.* Partially ordered state of ice XV. *Scientific Reports* **6,** 28920 (2016).

32. Giauque, W. F. & Stout, J. W. The Entropy of Water and the Third Law of Thermodynamics. The Heat Capacity of Ice from 15 to 273°K. *Journal of the American Chemical Society* **58,** 1144–1150. ISSN: 0002-7863. `http://pubs.acs.org/doi/abs/10.1021/ja01298a023` (1936).

33. Pauling, L. The Structure and Entropy of Ice and of Other Crystals with Some Randomness of Atomic Arrangement. *Journal of the American Chemical Society* **57,** 2680–2684. ISSN: 0002-7863. `http://pubs.acs.org/doi/abs/10.1021/ja01315a102` (1935).

34. Debye, P. Polar Molecules. *Dover Publ.* (1929).

35. Gasser, T. M. *et al.* Experiments indicating a second hydrogen ordered phase of ice VI. *Chemical Science* **9,** 4224–4234. ISSN: 20416539 (2018).

36. Pruzan, P., Chervin, J. C. & Gauthie, M. Raman spectroscopy investigation of ice vii and deuterated ice vi1 to 40gpa disorder in ice vii. *Epl* **13,** 81–87. ISSN: 12864854 (1990).

37. Pruzan, P., Chervin, J. C. & Canny, B. Stability domain of the ice VIII proton-ordered phase at very high pressure and low temperature. *The Journal of Chemical Physics* **99,** 9842–9846. ISSN: 00219606 (1993).

38. Caracas, R. & Hemley, R. J. Ferroelectricity in high-density H2O ice. *Journal of Chemical Physics* **142,** 134501–134507. ISSN: 00219606 (2015).

39. Pettinelli, E. *et al.* Reviews of Geophysics for subsurface radar exploration : A review. *Rev. Geophys.* **53,** 593–641 (2015).

40. Block, S., Weir, C. W. & Plermarini, G. J. High-pressure single-crystal studies of ice VI. *Science* **148,** 947–948. ISSN: 00368075 (1965).

41. Mishima, O., Môri, N. & Endo, S. Thermal expansion anomaly of ice VI related to the order-disorder transition. *The Journal of Chemical Physics* **70,** 2037–2038. ISSN: 00219606 (1979).

42. Johari, G. P. & Whalley, E. Evidence for a very slow transformation in ice VI at low temperatures. *The Journal of Chemical Physics* **70,** 2094–2097. ISSN: 00219606 (1979).

43. Salzmann, C. G., Radaelli, P. G., Mayer, E. & Finney, J. L. Ice XV: A new thermodynamically stable phase of ice. *Physical Review Letters* **103,** 105701. ISSN: 00319007 (2009).

44. Nanda, K. D. & Beran, G. J. What governs the proton ordering in ice XV? *Journal of Physical Chemistry Letters* **4,** 3165–3169. ISSN: 19487185 (2013).

45. Whale, T. F., Clark, S. J., Finney, J. L. & Salzmann, C. G. DFT-assisted interpretation of the Raman spectra of hydrogen-ordered ice XV. *Journal of Raman Spectroscopy* **44,** 290–298. ISSN: 03770486 (2013).

46. Shephard, J. J. & Salzmann, C. G. The complex kinetics of the ice VI to ice XV hydrogen ordering phase transition. *Chemical Physics Letters* **637,** 63–66. ISSN: 00092614. `http://dx.doi.org/10.1016/j.cplett.2015.07.064` (2015).

47. Del Ben, M., Vandevondele, J. & Slater, B. Periodic MP2, RPA, and boundary condition assessment of hydrogen ordering in ice XV. *Journal of Physical Chemistry Letters* **5,** 4122–4128. ISSN: 19487185 (2014).

48. Rosu-Finsen, A. & Salzmann, C. G. Origin of the low-temperature endotherm of acid-doped ice VI: New hydrogen-ordered phase of ice or deep glassy states? *Chemical Science* **10,** 515–523. ISSN: 20416539 (2019).

49. Thoeny, A. V., Gasser, T. M. & Loerting, T. Distinguishing ice β-XV from deep glassy ice VI: Raman spectroscopy. *Physical Chemistry Chemical Physics* **21,** 15452–15462. ISSN: 14639076 (2019).

50. Komatsu, K. *et al.* Development of a new P-T controlling system for neutron-scattering experiments. *High Pressure Research* **33,** 208–213. ISSN: 08957959 (2013).

51. Johari, G. P. Dielectric properties of ice VII and VIII and the phase boundary between ice VI and VII. *The Journal of Chemical Physics* **61,** 4292. ISSN: 00219606. `http://scitation.aip.org/content/aip/journal/jcp/61/10/10.1063/1.1681733` (1974).

52. Köster, K. W. *et al.* Dynamics enhanced by HCl doping triggers full Pauling entropy release at the ice XII-XIV transition. *Nature Communications* **6.** ISSN: 20411723 (2015).

53. Kubo, M. & Nakamura, S. The Dielectric Constant of Dispersion of Spherical Particles. *Bulletin of the Chemical Society of Japan* **26,** 318–322. ISSN: 0009-2673 (1953).

54. Whalley, E., Heath, J. B. & Davidson, D. W. Ice IX: An antiferroelectric phase related to ice III. *The Journal of Chemical Physics* **48,** 2362–2370. ISSN: 00219606 (1968).

55. Oguro, M. & Whitworth, R. W. Dielectric observations of the transformation of single crystals of KOH-doped ice Ih to ice XI. *Journal of Physics and Chemistry of Solids* **52,** 401–403. ISSN: 00223697 (1991).

56. Aroyo, M. I., Kirov, A., Capillas, C., Perez-Mato, J. M. & Wondratschek, H. Bilbao Crystallographic Server. II. Representations of crystallographic point groups and space groups. *Acta Crystallographica Section A: Foundations of Crystallography* **62,** 115–128. ISSN: 01087673 (2006).

57. Larson, A. C. & Dreele, R. B. V. *GSAS* tech. rep. (Los Alamos National Laboratory, New Mexico, USA., 2004).

58. Toby, B. H. EXPGUI, a graphical user interface for GSAS. *Journal of Applied Crystallography* **34,** 210–213. ISSN: 00218898 (2001).

59. Salzmann, C. G. *et al.* Detailed crystallographic analysis of the ice VI to ice XV hydrogen ordering phase transition. *Journal of Chemical Physics* **145,** 204501. ISSN: 00219606 (2016).

60. Knight, C. & Singer, S. J. Hydrogen bond ordering in ice v and the transition to ice XIII. *Journal of Chemical Physics* **129.** ISSN: 00219606 (2008).

61. Klotz, S. *et al.* Bulk moduli and equations of state of ice VII and ice VIII. *Physical Review B* **95,** 174111. ISSN: 24699969 (2017).

62. Benoit, M., Bernasconi, M., Focher, P. & Parrinello, M. New High-Pressure Phase of Ice. *Physical Review Letters* **76,** 2934–2936. ISSN: 10797114 (1996).

63. Somayazulu, M. *et al.* In situ high-pressure x-ray diffraction study of H2 O ice VII. *Journal of Chemical Physics* **128.** ISSN: 00219606 (2008).

64. Fukui, H., Hiraoka, N., Hirao, N., Aoki, K. & Akahama, Y. Suppression of X-ray-induced dissociation of H2O molecules in dense ice under pressure. *Scientific Reports* **6,** 2–10. `http://dx.doi.org/10.1038/srep26641` (2016).

65. Okada, T., Iitaka, T., Yagi, T. & Aoki, K. Electrical conductivity of ice VII. *Scientific Reports* **4,** 5778. ISSN: 2045-2322. `http://www.pubmedcentral.nih.gov/articlerender.fcgi?artid=4105784&tool=pmcentrez&rendertype=abstract%5Cnhttp://www.nature.com/articles/srep05778` (2014).

66. Noguchi, N. & Okuchi, T. Self-diffusion of protons in H2O ice VII at high pressures: Anomaly around 10 GPa. *Journal of Chemical Physics* **144,** 234503. ISSN: 00219606 (2016).

67. Weissmann, M. & Cohan, N. V. Molecular Orbital Study of Ionic Defects in Ice. *The Journal of Chemical Physics* **43,** 124–126. ISSN: 0021-9606. `http://aip.scitation.org/doi/10.1063/1.1696439` (1965).

68. Minceva-Sukarova, B., Sherman, W. F. & Wilkinson, G. R. The Raman spectra of ice (Ih, II, III, V, VI and IX) as functions of pressure and temperature. *Journal of Physics C: Solid State Physics* **17,** 5833–5850. ISSN: 00223719 (1984).

69. Pruzan, P. *et al.* Phase diagram of ice in the VII-VIII-X domain. Vibrational and structural data for strongly compressed ice VIII. *Journal of Raman Spectroscopy* **34,** 591–610. ISSN: 0377-0486. http://doi.wiley.com/10.1002/jrs.1039 (2003).

70. Hirai, H., Kadobayashi, H., Matsuoka, T., Ohishi, Y. & Yamamoto, Y. High pressure X-ray diffraction and Raman spectroscopic studies of the phase change of D2O ice VII at approximately 11 GPa. *High Pressure Research* **34,** 289–296. ISSN: 14772299. https://doi.org/10.1080/08957959.2014.913041 (2014).

71. Booth, N. *et al.* Three impossible things before lunch – the task of a sample environment specialist. *Journal of Neutron Research* **19,** 49–56. ISSN: 14772655. http://www.medra.org/servlet/aliasResolver?alias=iospress&doi=10.3233/JNR-170041 (2017).

72. Whalley, E., Davidson, D. W. & Heath, J. B. Dielectric properties of ice VII. Ice VIII: A new phase of ice. *The Journal of Chemical Physics* **45,** 3976–3982. ISSN: 00219606 (1966).

73. Klotz, S. *Techniques in High Pressure Neutron Scattering* 1st, 276 (CRC Press, 2016).

74. Aoyama, T. *et al.* Giant spin-driven ferroelectric polarization in TbMnO3 under high pressure. *Nature Communications* **5,** 4–10. ISSN: 20411723 (2014).

75. Iizuka, R., Yagi, T., Gotou, H., Komatsu, K. & Kagi, H. An opposed-anvil-type apparatus with an optical window and a wide-angle aperture for neutron diffraction. *High Pressure Research* **32,** 430–441. ISSN: 0895-7959. http://www.tandfonline.com/doi/abs/10.1080/08957959.2012.722213 (2012).

76. Shin, D., Hwang, J. & Jhe, W. Ice-VII-like molecular structure of ambient water nanomeniscus. *Nature Communications* **10,** 1–8. ISSN: 20411723. http://dx.doi.org/10.1038/s41467-019-08292-0 (2019).

77. Algara-Siller, G. *et al.* Square ice in graphene nanocapillaries. *Nature* **519,** 443–445. ISSN: 14764687 (2015).

78. Tschauner, O. *et al.* Ice-VII inclusions in diamonds: Evidence for aqueous fluid in Earth's deep mantle. *Science* **359,** 1136–1139. ISSN: 10959203 (2018).